HYBRID JOINING IN AUTOMOTIVE APPLICATIONS

Vlastimil Kunc
Oak Ridge Associated Universities
Oak Ridge, TN 37830

Donald Erdman, Lynn Klett
Oak Ridge National Laboratory
Oak Ridge, TN 37831

ABSTRACT

The objective of the ongoing Hybrid Joining Project, funded as part of the Automotive Lightweighting Materials Program, is to develop new experimental methods and analysis techniques to enable hybrid joining to become a viable attachment technology in automotive structures. This will be accomplished by evaluating the mechanical behavior of a representative structure consisting of a composite hat section attached to a metal sheet under bending loads. Three attachment methods are evaluated including riveting, adhesive bonding, and combination of riveting and adhesive bonding. Experimental results for quasi-static, fatigue and creep tests are presented. Quasi-static tests were conducted at room temperature and at -40°C. Joint failure was not observed for the quasi-static tests, however the attachment technique affected both the stiffness and failure mode of the structure. Some specimens incurred significant joint damage in the fatigue tests prior to catastrophic failure. Finite element models (FEM) can currently predict the behavior of the structure up to the point of damage in the composite. Comparison of experimental results and FEM is presented. The results and observations obtained from this project will facilitate incorporation of lightweight composite materials into automotive structures. Innovative design using dissimilar materials and effective joining techniques will result in reduced vehicle weight and fuel consumption.

KEY WORDS: composite structures, hybrid joining, adhesive bonding

1. INTRODUCTION

Weight can be reduced and fuel efficiency increased in automobiles, without compromising structural integrity or utility, by incorporating innovative designs that strategically utilize modern lightweight materials—such as polymeric composites—in conjunction with traditional structural materials such as aluminum, magnesium and steel. Despite the advantages associated with such dissimilar or hybrid material systems, there is reluctance to adopt them for primary structural applications. In part, this reluctance can be attributed to the limited knowledge of joining

techniques with such disparate materials where traditional fastening methods such as welding, riveting, screw-type fasteners, and bolted joints may not be appropriate.

One solution to this problem is the use of hybrid joining techniques by which a combination of two or more fastening methods is employed to attach similar or dissimilar materials. One example is a mechanically fastened joint (i.e., bolted or riveted) that is also bonded with adhesive (1). These types of joints could provide a compromise between a familiar mechanical attachment that has proven reliability, and the reduction of problematic issues such as stress concentrations and crack nucleation sites introduced by using mechanical fasteners with polymeric composites.

The use of hybrid joining could also lead to other benefits such as increased joint rigidity, contributing to overall stiffness gains and a reduction of vehicle mass (2,3,4). Additionally, the use of adhesives in conjunction with mechanical fasteners could significantly reduce stress concentrations, which serve as locations for crack starters. Hybrid joining methods can also provide additional joint continuity to allow increased spacing between fasteners or welds.

Although numerous benefits are derived from the utilization of hybrid joining techniques, and the joining of dissimilar materials is becoming a reality, little or no practical information is available concerning the performance and durability of hybrid joints. Therefore this project has taken on the task of developing new technologies to quantify joint toughness and predict long-term durability. This necessitates identifying and developing an understanding of key issues associated with hybrid joint performance, such as creep, fatigue, and effects of environmental exposure.

To initiate this study, it was necessary to choose a candidate hybrid joint representative of those typically encountered in automobiles. Because of the wide applicability in automotive structures, several combinations of hat section geometries were considered. Hat sections can be incorporated into a variety of generic automotive structural components, such as crush-tubes or frame rails, when they are bonded and mechanically fastened to other components. A composite hat section bonded and riveted to a steel base was selected for the current study. To determine the influences of the adhesive and the rivets on the structural performance of the rail, bonded specimens without rivets and riveted specimens without adhesive were also investigated.

2. MATERIALS

The specimens under consideration consist of a composite hat and steel plate fastened with adhesive and/or rivets. Large flange 4.7625 mm diameter (3/16 in.) open end blind rivets made by Textron were supplied by DaimlerChrysler (part# 06035255). Epoxy adhesive PL 731 was supplied by SIA Adhesives Inc. (5), and was applied in 0.25 mm thickness. Cold rolled, galvanized mild steel 1020 of 1 mm thickness, made by US Steel, was joined to composite hat sections. These hat sections were either e-glass swirled mat/urethane matrix provided by the Automotive Composites Consortium, or short carbon fiber composite AMC 8590 supplied by Quantum Composites. The swirled mat composite has been thoroughly characterized in previous studies (6,7). Properties of the Quantum composite and the adhesive were evaluated as a part of this project.

Quantum Composite Material

Coupon tensile testing was performed to characterize the Quantum carbon fiber composite material, which was used for the most recent set of hat section specimens comprising the hybrid joint rail under consideration. Upon exploratory tensile testing of flat coupon specimens, substantial variations in stiffness and strength properties were discovered. Therefore, a large number of tests was performed to statistically quantify the material properties for use in structural modeling of the rails.

Stiffness was measured on 12.7 mm (0.5 in.) wide tensile specimens using an extensometer with a 25.4 mm (1-in.) gage length. Stiffness measurements varied among replicate specimens as well as at various extensometer locations on a single specimen (Figure 1). Similar behavior was observed for other types of chopped carbon fiber composite [8]. Incremental loading tests were carried out to assess material property degradation as a function of applied stress. For these incremental loading tests, tensile specimens were subjected to monotonically increasing load cycles in an attempt to observe a global indication of damage progression through reduction of stiffness. To achieve this goal, tensile coupons were loaded in 889.64 KN (200 lb) increments and the average of three stiffness measurements after each loading cycle was recorded. A modest decrease in Young's modulus was observed with increased load level as shown in Figure 2. The outlier at approximately 3000 N may be attributed to the non-homogenous properties of the material. For example, the primary damage during the incremental loading was usually associated with broken fibers and cracked matrix material, and this may take place outside the gage length of the extensometer at a relatively weaker location. If the damage outside the gage length is localized in such a region, it most likely will not be detected from the stiffness measurement.

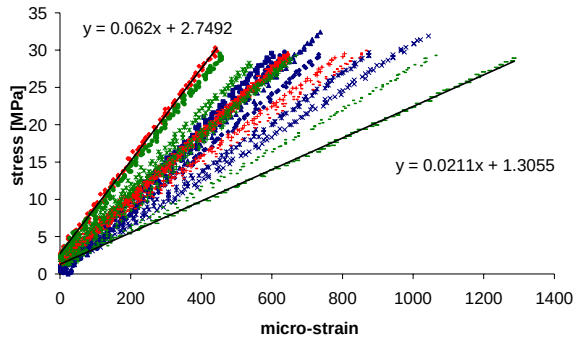

Figure 1. Stress-strain curves at six locations for three Quantum tensile specimens (identified by color).

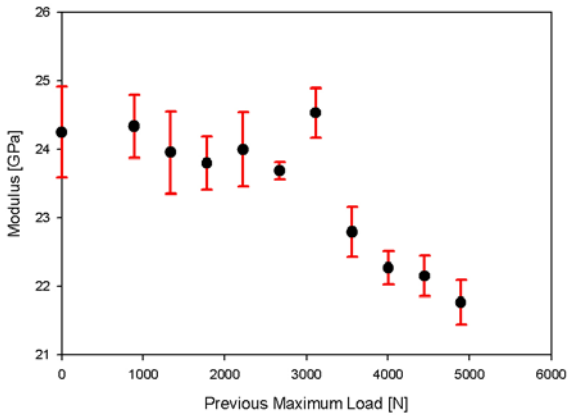

Figure 2. Decrease in stiffness of incrementally loaded Quantum specimen.

Epoxy Adhesive PL 731 SI

The material data sheet (5) provided by the manufacturer did not provide the modulus or Poisson's ratio of the adhesive necessary to accurately model the behavior of the adhesive. Therefore, plates of cured adhesive were cut into 12.7 mm (0.5 in.) wide dog-bone tensile

specimens. After assessing the results of a set of tensile tests, severe inconsistencies were found in the data. Examination of the fracture surfaces for suspect specimens, which exhibited lower than average strength and/or stiffness measurements, often had large voids attributed to trapped gasses introduced during the molding process. These voids are easily discernable with the naked eye as shown in Figure 3. These bubbles provided crack starter sites, and effectively reduced the cross-sectional area of the specimen, resulting in the aforementioned inconsistencies. To eliminate the voids, a new procedure was developed to deposit the highly viscous adhesive onto the molding platens after centrifuging to remove any air introduced in the mixing process. Any manipulation of the adhesive, which would result in shearing or tensile forces, was eliminated and only compressive forces were used to distribute the adhesive to fill the mold. The specimens machined from the plaques molded in this manner were significantly more homogenous and void free. Furthermore, post-test examination of the fracture surfaces indicated failure of the material that was not initiated from voids in the material, resulting in much more consistent stress-strain behavior as depicted in Figure 4 with the corresponding material properties shown in Table 1. This processing technique was adopted for preparing all further adhesive tensile and creep test specimens.

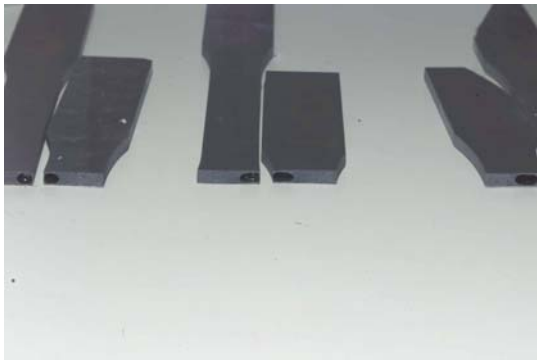

Figure 3. Internal bubbles/voids on tensile specimen fracture surfaces attributed to inaccuracies and scatter in material properties.

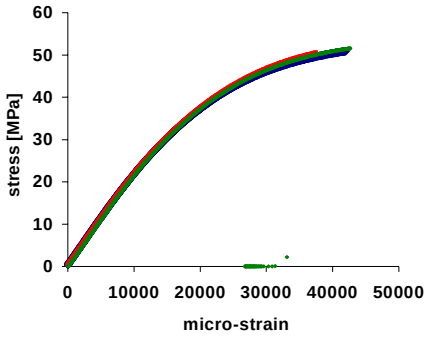

Figure 4. Typical stress-strain curves with the new specimen processing techniques showing reduced scatter.

Table 1. Static test properties for the specimens from Figure 4.

	Strength [MPa]	Modulus [GPa]
Average	50.986	2.253
Standard Deviation	0.503	0.004

Adhesive Creep Testing

Due to the time dependent response of adhesives under constant load, the sensitivity of the rail specimens to adhesive creep was established for the modeling effort. The first step was to carry out creep testing on tensile specimens and determine the strain accumulation over a period of time. Typical creep curves are plotted in Figure 5 for an initial stress level equal to 60% of the failure stress. Although there is noticeable scatter in the curves (variation in strain level with

identical stress levels), this data could be used within the FEM model to determine if the creep response of the adhesive made a significant contribution to the overall response of the rail. The creep data was then curve fitted with a standard power-law representation suitable for the FEM program (ABAQUS) input:

$$\varepsilon_{creep} = C\sigma t^{n} \quad [1]$$

Where:

$$\varepsilon_{creep} = creep\ strain$$
$$\sigma = applied\ \ stress$$
$$t = time$$
$$C, n = power\ law\ coefficients$$

Since the applied stress and the time were known, simple curve fitting techniques were used to determine the coefficients for the power law (C=0.0012, n=0.17). The creep strain, which increases with time, was then added to the instantaneous strain obtained at the start of the test to obtain the total strain. This information was then input in the rail model, with similar creep properties for the composite (6,7).

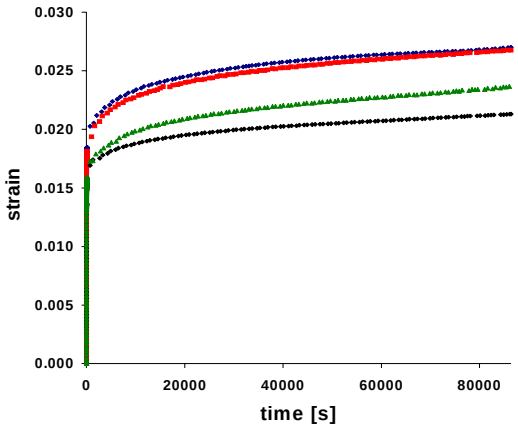

Figure 5. Creep test data for four adhesive specimens at 60% of failure stress exhibiting noticeable scatter.

3. EXPERIMENTAL

Experimental Setup

The rail specimens were tested in three point bending with two configurations. In the first configuration, the top of the composite hat was in tension. The center loading point consisted of a 50.8 mm (2 in.) diameter roller, and the supports were 16.51 cm (6.5 in.) diameter rollers supporting the flanges 20.32 cm (8 in.) from the center. This configuration, depicted in Figure 6,

will be referred to as "hat in tension". The "hat in compression" fixture consists of two 50.8 mm (2 in.) diameter rollers loading the flanges at the center of the specimen. The supports are 25.4 mm (1 in.) diameter bars 20.32 cm (8 in.) from the center. This setup is depicted in Figure 7.

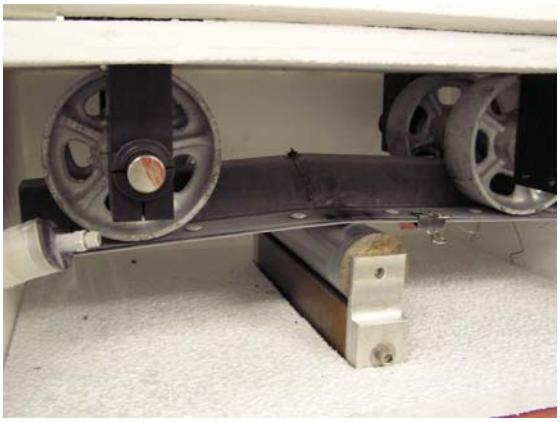

Figure 6. Load fixture for hat in tension.

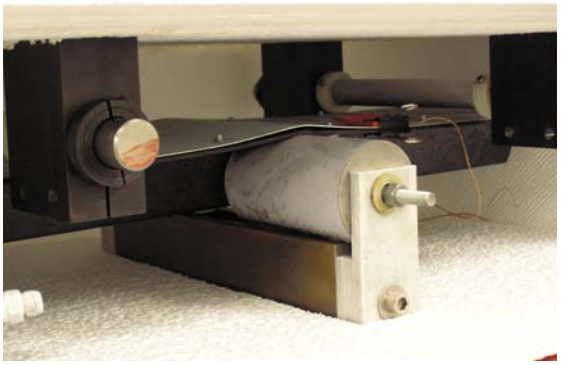

Figure 7. Load fixture for hat in compression.

Results for Glass Hats

Preliminary tests were conducted on rail specimens with swirled glass mat/urethane matrix composite hats. Ultimate loads at failure for a full set of quasi-static tests, conducted at room temperature with a load rate of 0.04233 mm/s (0.1 in./min) in stroke control, are presented in Table 2. For several of these tests, the specimens were instrumented with linear variable differential transformers, or LVDTs, placed 101.6 mm (4 in.) from the center roller (Figure 8).

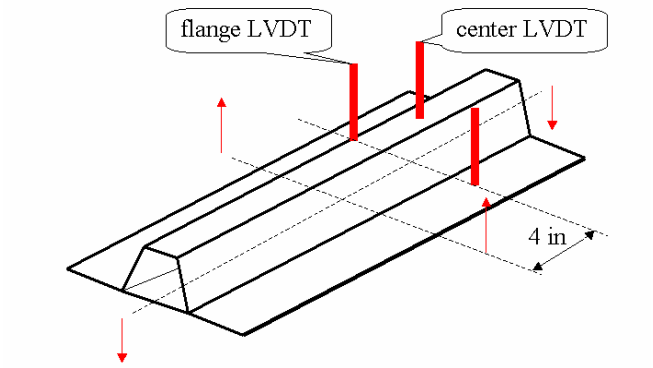

Figure 8. Schematic drawing of hat in tension instrumented with three LVDTs.

Table 2. Average maximum load obtained from three sets of quasi-static tests for glass/urethane.

Maximum Load [kN]	tension	compression
Rivets and Adhesive	15.7	17.7
Rivets	14.0	8.15
Adhesive	17.7	12.5

Although there was no detectable damage in the joint for the hat in tension rail specimens, the joining technique had a significant effect on the failure process. Joints containing adhesive (adhesive only, and adhesive with rivets) failed suddenly and catastrophically at the top of the hat. Typical load-displacement behavior for different specimens as well as results from the FEM are shown in Figure 9. The primary source of non-linearity is not damage in the structure, but rather the geometry changes resulting from the specimen deformation during the test. Specimens with rivets only grew a crack from the flange up, until the crack reached the top of the hat and the specimen collapsed. The damage is indicated by a drop in the load and irregularities in the latter part of the load-displacement curve. All specimens developed permanent saddle-like deformation in the steel and exhibited lifting of flanges from the center roller during the test.

The failure mechanism for specimens loaded with hat in compression was identical for all three joining techniques. Initial elastic loading was followed by plastic deformation in the metal. Loading continued until the flanges tore from the hat at the contact location with the center rollers. This damage was accompanied by a discernable drop in the load. Subsequent increases in displacement resulted in an irregular but essentially constant load due to tearing of flanges from the hat. This load-displacement behavior as well as the FEM results are shown in Figure 10.

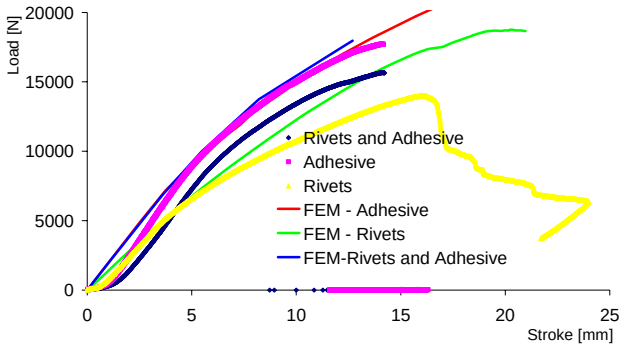

Figure 9. Load-displacement behavior for hat in tension rail specimens.

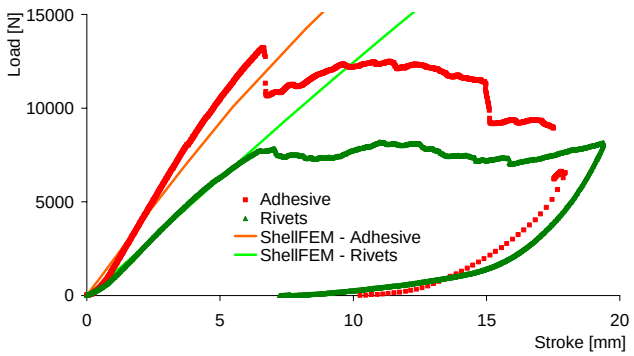

Figure 10. Load-displacement behavior for hat in compression rail specimens.

Creep tests at 85% of ultimate load were conducted in addition to the quasi-static tests to assess the overall creep characteristics of the structure and for comparison with the finite element model.

Finite Element Analysis

Finite element models were developed using Abaqus 6.2 by HKS Inc. and compared to the experimental results. Models with solid hexahedron elements as well as four-sided shell elements were examined. Both models assume isotropic elastic-perfectly plastic behavior for the metal, and elastic behavior for both the joint (adhesive or rivets) and the composite. Material property values used in the analyses are listed in Table 3. The non-linear geometry option was used (9) to capture the effects of specimen deflection on the loading geometry. The contact between the rollers and the specimen as well as between the composite hat and metal (rivets only) was simulated using the master-slave algorithm. Solid elements were used for the hat in tension analysis, while shell elements with tied nodes in place of rivets were used in the hat in

compression analysis. These models match the experimental results up to the point where significant damage in the composite occurs (Figures 9 and 10). Additionally there is good correlation between the model predictions and the results from LVDTs as shown in Figure 11.

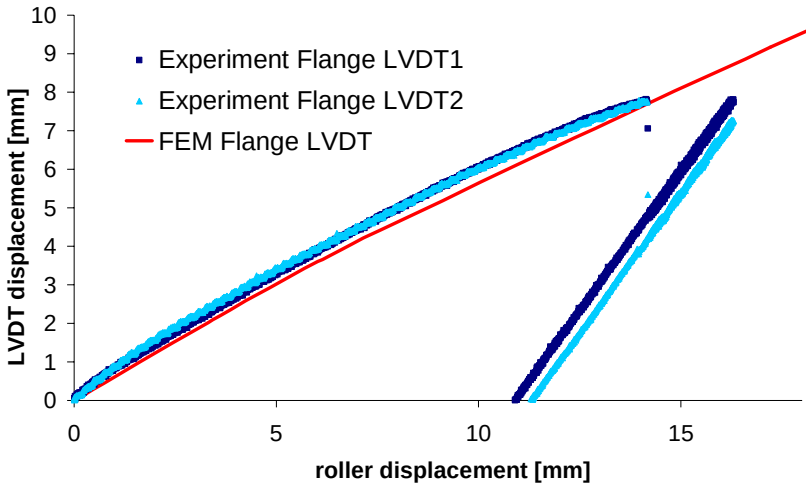

Figure 11. Load-displacement results for FEM compared to experimental data for hat in tension test.

Table 3. Material properties for FEM.

Material	Young's Modulus [GPa]	Poisson's Ratio	Yield Stress [MPa]
Composite	10.34	0.33	N/A
Adhesive	2.253	0.4	N/A
Mild Steel	206.8	0.3	137.8

A creep analysis on the complete rail was carried out in three steps, first considering only creep of the adhesive, only creep of the glass composite, and finally with creep behavior included for both the composite and the adhesive. Four-sided shell elements were used for this analysis. The results for these cases are plotted in Figure 12. Although the neat adhesive exhibits significant creep response (Figure 5), the effect is negligible on the overall rail response. However, including the creep response of the glass composite results in substantial creep of the rail. Therefore, the additional computation to include the creep response of the adhesive is unnecessary and can be omitted in future model development to streamline the final durability predictions. The FEM results were compared to a creep test on a glass-composite rail specimen (Figure 13). There are large discrepancies between the model and the experimental results except at the start of the test. This is not surprising considering the large amount of obvious damage observed during the test that is not included in the current model. It should be noted, however, that the test on the rail specimen was run at 85% of failure load which resulted in the large damage accumulation indicated by the periodic jumps in strain level over time. Several smeared-damage models were investigated, but none of them accurately represented the experimental results. In spite of this shortcoming, finite element analyses revealed the following:

-It is possible both to accurately model the behavior of the structure up to the point of significant damage in the composite with a relatively simple model and to capture the difference in global load-displacement behavior due to the joining techniques.
-Shell elements can be used to predict the global behavior at significantly smaller computational expense without sacrificing accuracy.
- FEM predicted lifting of flanges at the center roller, which was later observed in the tests in addition of the saddle-like permanent deformation of the steel observed during the experiments.
-Creep in the composite hat dominates the creep response of the structure. Creep in the adhesive is of negligible importance for the global response.

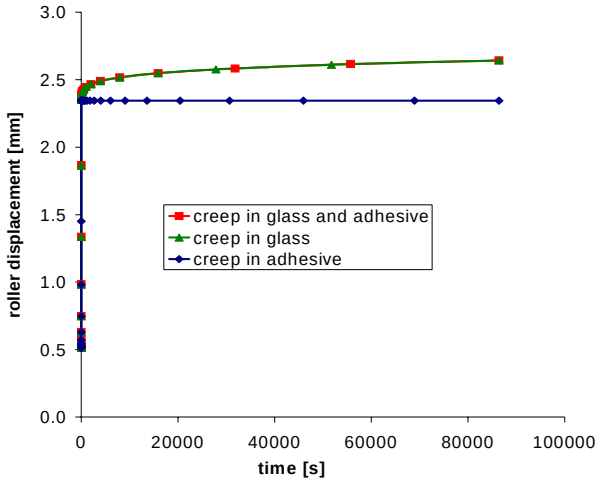

Figure 12. FEM creep sensitivity results for a glass rail specimen.

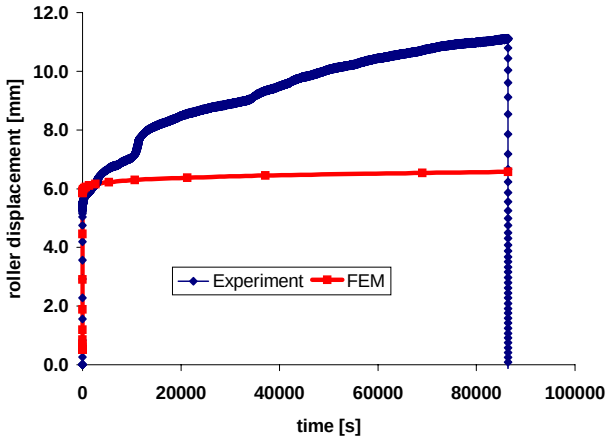

Figure 13. FEM creep results compared with experimental creep data for a glass rail specimen.

Results for Quantum Hats

Quasi-static, fatigue and creep tests of rail specimens with Quantum composite hats were conducted to assess their mechanical performance and provide validation for future modeling. Joining methods were consistent with previous rail tests conducted on swirled mat glass specimens. Namely the three cases of the specimens joined via adhesive bonding, riveting and a combination of riveting and bonding were revisited. The loading conditions were also adopted from previous studies, namely with the hat section being loaded in both tension and compression.
Quasi-static tests at room temperature

Three replicate specimens were tested for each combination of loading (tension and compression) and each joint configurations. Two of the three replicate tests were instrumented with LVDTs for the hat in tension, and a single displacement gage for the hat in compression. The results from these displacement measurements will be used to correlate with the predicted displacements from analytical models.

Damage and failure behavior observed during the quasi-static tests of the Quantum hat section specimens was somewhat similar to that observed for previous swirled-mat-glass hat section specimens indicating the damage characteristics are probably dictated more by the geometry of the specimen than the properties of the composite material.

For the hat in tension specimens, catastrophic failure occurred at the top of the hat section and remained solely in the composite material. The crack was often located away from the longitudinal center of the specimen where the bending stresses were maximum, likely because of the property variation in the Quantum material (Figure 14). Hence, the specimen failed at a location where the stresses were lower, but where the material strength was also lower. Unlike for swirled glass hats, there was no difference between the failure mechanism for specimens with different joints. Only two specimens sustained significant push-through damage from contact stresses of the rollers initiating cracks starting at the flange and influencing the load-displacement behavior.

A brief summary of the maximum loads for the tests carried out on the Quantum composite rail specimens is presented in Table 4. It is interesting to note that the loads attained are consistently higher for the joints that are both bonded and riveted giving an indication that a single joining method may be inferior to the hybrid joints utilizing both mechanical attachment and adhesive bonding. Alternatively, the higher ultimate loads could be attributed to variations in material properties.

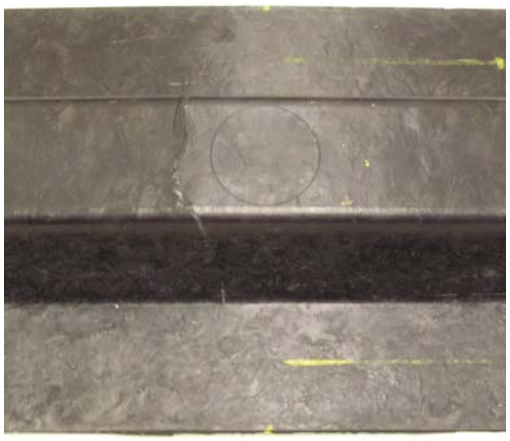

Figure 14. Adhesively bonded specimen after quasi-static test with hat in tension exhibiting off-center failure.

Table 4. Average maximum load obtained from three sets of quasi-static tests for Quantum hat section specimens.

Average Maximum Load [kN]	tension	compression
Rivets and Adhesive	18.0	18.6
Rivets	13.8	15.6
Adhesive	17.0	15.6

Fatigue tests at room temperature

Fatigue tests on three replicates of each specimen configuration were performed at 70% of ultimate load determined from the average of the quasi-static tests for each loading/joint attachment configuration. As with most S-N fatigue testing, an order of magnitude difference in the number of cycles to failure for replicate fatigue tests was observed. Specimens failing at lower number of cycles generally sustained damage comparable to the specimens tested in quasi-static mode indicating weak regions in the hat sections, which was not surprising considering the variability of composite strength and stiffness among the various specimens and within the specimen itself. Specimens failing at higher cycle counts exhibited extensive progressive damage including multiple rivet failures, widespread adhesive cracking, and cracks originating from areas of high stress and rivet holes, which progressed to the extent that cracks were developed and grew in the metal base of the specimen prior to failure.

Of the three specimens tested with hat in tension with adhesive and rivets, one exhibited cracking in the metal. This specimen carried load for 98,820 cycles, compared to 11,100 and 7,600 cycles for the specimens which failed in the composite before any damage developed in other parts of the structure. The same scenario applies to hat in tension with rivets only. One specimen lasted for 286,500 cycles with rivets starting to fail at approximately 120,000 cycles. The other two specimens, with fatigue lives of 35,400 and 44,000 cycles, failed suddenly in the composite. None of the three specimens with the hat in tension and adhesive only developed detectable damage before final failures at 3,100, 26,200, and 52,000 cycles.

This failure behavior can be explained by the large variation in strengths and stiffness observed in the Quantum material. When the highly stressed areas of the specimen coincided with weak material areas in the composite hat, the hat failed in these regions in a manner similar to the quasi-static tests. When the material in highly stressed areas of the hat was strong enough to sustain the fatigue loading without immediate failure, other components of the structure failed and re-distributed the stresses enabling the structure to sustained a much greater level of damage prior to collapse. Examples of these types of extensive damage are shown in Figures 15 and 16 where numerous rivet pullouts and extensive cracking of the metal base can be readily observed.

Results for specimens tested with hat in compression are more consistent. All three specimens with adhesive only developed cracks in the metal. The cycles to catastrophic failure were 481,100, 307,100, and 175,700. Crack initiation and propagation can be detected from the global response of the structure as shown in Figures 17 and 18. All specimens with hat in compression with rivets only exhibited rivet failure leading to redistribution of load to the composite hat. Eventually the hat failed in the flanges as well as the sides of the hat at 43,200, 52,600 and 151,100 cycles. At this point, the top of the hat hit the support of the bending fixture indicated by an increase in stiffness since the fixture was effectively carrying the load. Specimens with rivets and adhesive did not fail catastrophically, instead the flanges were torn away from the hat in the same manner as observed in the quasi-static tests. It took 45,000, 45,000 and 92,000 cycles for the flanges to tear enough to allow the top of the hat to reach the support of the bending fixture. One specimen developed cracks in the metal while another developed cracks in the adhesive.

Figure 15. Broken and missing rivets in riveted specimen that failed after 43,200 cycles at 70% of static ultimate load with the hat in compression.

Figure 16. Cracking of steel during fatigue test for adhesively bonded specimen that failed at 307,100 cycles at 70% of static ultimate load with hat in compression.

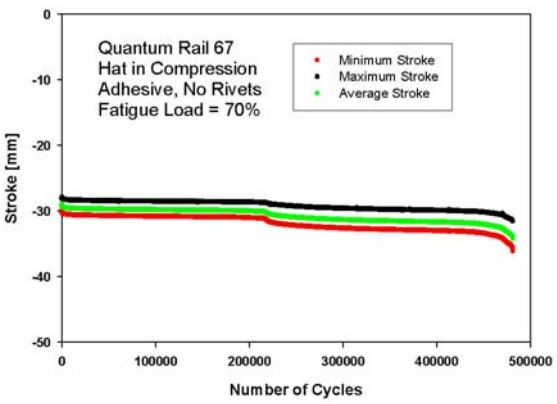

Figure 17. Typical fatigue behavior of specimen with adhesive only, hat in compression. Onset of crack in the metal is noticeable at 230,000 cycles.

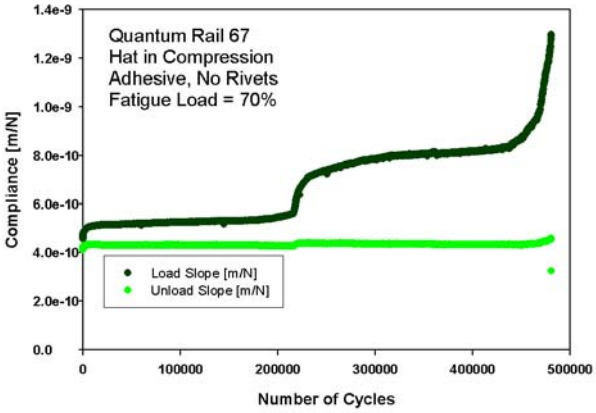

Figure 18. Typical compliance behavior for specimen with adhesive only, hat in compression. Onset of crack in the metal is clearly recognizable at 230,000 cycles.

Creep tests at room temperature

A complete permutation of the three specimen types and the two loading conditions were included in the creep test matrix. Specimens were tested for creep at 40% of ultimate load level to avoid large-scale damage since the viscoelastic response of the material was needed for modeling efforts that do not currently contain damage analysis. The load was applied to the specimen in a ramp lasting one second for a period of one day. Then the load was removed in one second ramp, and recovery of the specimen was observed for an additional day. There was no visible damage on the Quantum hats, although occasionally imprints from the rollers were detectable in the steel substrate of the structure. Minor matrix cracking could be heard on initial loading for some specimens, indicating minimal damage in the composite. Hence, the time dependent increase in displacements recorded throughout the creep test (Figure 19) were believed to be caused by the time dependent material response and not by extensive damage which would be indicated by large jumps in displacement at intermittent points in the test. The level and significance of any indiscernible damage could possibly be estimated by evaluating the

residual deformation after unloading and comparing the test results to time dependent finite element simulations, which do not include damage. Comparisons of the creep curve with finite element models are currently underway.

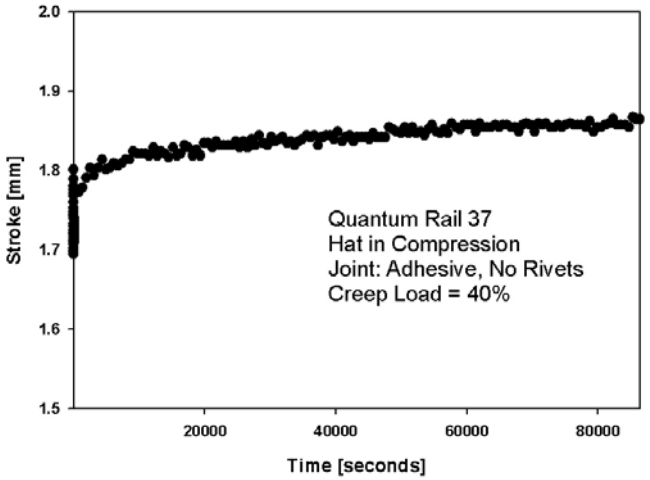

Figure 19. Representative creep curve for adhesively bonded hat in compression.

Quasi-static tests at -40°C

A set of quasi-static tests was carried out at -40°C. An in-house designed Styrofoam environmental chamber was cooled with liquid nitrogen to -40°C. Sufficient time was allowed to reach equilibrium state and achieve a uniform specimen temperature. The test was carried out in the same manner as the quasi-static test at room temperature (loading rate 0.04233 mm/s - 0.1 in./min). The major difference in the results for the cold testing was a general increase in the load at failure (Table 5) compared to the room temperature testing. Although bond failure was observed for some adhesively bonded specimens, it is unclear if the failure occurred during the test or after the composite failure, since the specimen could not be visually observed inside the chamber during the test. The increase in strength in the cold condition may be attributed to the increase in stiffness of composite material leading to smaller displacements and possibly accompanied by a higher yield point in the steel. Nevertheless, for static strength concerns, the cold environment did not appear to have a detrimental effect on the strength of the structure.

Table 5. Maximum load for quasi-static tests at -40°C.

maximum load [kN]	tension	compression
rivets and adhesive	20.73	20.00
rivets	15.70	17.79
adhesive	16.79	21.37

4. CONCLUSIONS

This research has revealed some complexities of joining dissimilar materials. Structures consisting of composite hat sections joined to a sheet of metal by riveting, adhesive bonding, or combination of both were tested in three point bending with hat in tension or hat in compression.

Joint failure was not observed for quasi-static tests at room temperature. However the type of joint influenced the failure behavior of the specimens with swirled glass hat section. Study of specimens with chopped carbon fibers is complicated by the non-homogeneous elastic properties of the material on macroscopic scale, which caused off-center failures in the quasi-static tests and inconsistent failure mechanisms for the fatigue tests. Rivet failure and metal cracking were observed in fatigue tests for specimens with higher fatigue life. Specimens tested at -40°C failed at higher loads than at room temperature.

Creep tests at 85% of ultimate load were dominated by damage in the composite. At 40% of ultimate load, the carbon composite specimens sustained negligible damage, with obvious evidence of viscoelastic response.

Finite element models accurately represent global static behavior of the specimens up to the point of significant damage in the composite. Models also revealed that creep in the composite drives the visco-elastic behavior of the structure with the swirled glass hat, while creep in the adhesive can be neglected without sacrificing accuracy of the global response. Further characterization of Quantum composite material properties is necessary in order to develop models accurately representing the behavior of the hat section/steel structure. Further experiments will be conducted on the rail specimens to evaluate performance in various environments.

5. ACKNOWLEDGEMENTS

This research is sponsored by the U.S. Department of Energy, Assistant Secretary for Energy Efficiency and Renewable Energy, Office of FreedomCAR and Vehicle Technologies, as part of the Automotive Lightweighting Materials Program, under contract DE-AC05-00OR22725 with ORNL operated by UT-Battelle, LLC for the U.S. Department of Energy. The authors would like to thank Rick Battiste and Ronny Lomax of Oak Ridge National Laboratory as well as the Joining Task Force of the Automotive Composites Consortium for their valuable contributions to this research.

6. REFERENCES

1. J. Liu and T. Sawa, J Adhes. Sci. Technol., 15 (1), 43 (2001).
2. T. Kobayashi and T. Matsubayashi, JSME International Journal, 34 (4), 526 (1991).
3. T. Pine, M. M. K. Lee, and T. B .Jones, Ironmaking and Steelmaking, 25 (3), 205 (1998).
4. T. Pine, M. M. K. Lee, and T. B. Jones, Proceedings of the Institution of Mechanical Engineers, Part D: Journal of Automobile Engineering, 214 (4), 347 (2000).
5. Epoxy PL 731SI Product Data Sheet, SIA Adhesives, Inc. (2003).
6. J. M. Corum, et.al., "Durability-Based Design Criteria for a Chopped-Glass-Fiber Automotive Structural Composite," ORNL/TM-1999/182, November 1999.
7. L. V. Smith and Y. J. Weitsman, “The Visco-Damage Mechanical Response of Swirl-Mat Composites," ORNL/TM-13281, September 1996.
8 J. M. Corum, et. al., "Durability-Based Design Criteria for a Chopped-Carbon-Fiber Automotive Composite," ORNL/TM-2003/86, May 2003.
9 Abaqus Documentation, Hibbitt, Karlsson & Sorensen, Inc. (2001).